Proceedings of the 34th International Symposium on Combustion. Warsaw, Poland July 29- August 3. 2012
Published in Proceedings of the Combustion Institute, Vol. 34, pp. 895-902, 2012.

# Experimental Study of Minimum Ignition Energy of Lean $H_2$-$N_2O$ Mixtures

S. CORONEL[a], R. MÉVEL[a], S.P.M. BANE[b], J.E. SHEPHERD[a]

[a] Graduate Aerospace Laboratories, California Institute of Technology
1200 E. California Blvd, Pasadena, California 91125, USA

[b] School of Aeronautics and Astronautics, Purdue University
701 West Stadium Avenue, West Lafayette, Indiana 47907, USA

## Abstract

Ignition energies for short duration (<50 ns) spark discharges were measured for undiluted and nitrogen-diluted $H_2$-$N_2O$ mixtures of equivalence ratios $\phi$ = 0.15 and 0.2, dilution of 0% and 20% $N_2$, and initial pressures of 15 – 25 kPa. The ignition events were analyzed using statistical tools and the probability of ignition versus spark energy density (spark energy divided by the spark length) was obtained. The simple cylindrical ignition kernel model was compared against the results from the present study. Initial pressure has a significant effect on the width of the probability distribution, ranging from a broad (P = 15 kPa) to a narrow (P = 25 kPa) probability distribution indicating that the statistical variation of median spark energy density increases as initial pressure of the mixture decreases. A change in the equivalence ratio from 0.15 to 0.2 had a small effect on the median spark energy density. The addition of 20% $N_2$ dilution caused a significant increase in the median spark energy density when compared to no dilution. The extrapolation of the present results to atmospheric pressure, stoichiometric $H_2$-$N_2O$ indicates that the electrostatic discharge ignition hazards are comparable to or greater than $H_2$-$O_2$ mixtures.

Keywords: Spark Ignition; Minimum ignition energy; Hydrogen; Nitrous oxide; Nuclear waste safety.

## 1. Introduction

The Hanford site, located in south central Washington, has been used for more than 40 years to produce plutonium for the United States' nuclear weapons arsenal. This led to the largest amount of localized nuclear waste in the United States. Since plutonium production in the United States ceased in the late nineteen eighties, the Hanford site has been engaged in a waste cleanup phase that will extend several more decades [1,2]. The stored waste at the facility continuously generates gaseous compounds that form mixtures of $H_2$, nitrous oxide ($N_2O$), $O_2$, $N_2$, ammonia ($NH_3$) and methane ($CH_4$) [3]. The hazard related to the accidental ignition of these gas mixtures must therefore be considered, particularly that of hydrogen-nitrous oxide ($H_2$-$N_2O$) mixtures.

Over the past 20 years, numerous studies have been conducted to characterize the explosive properties of $H_2$-$N_2O$. Pfahl et al. studied the flammability limits of $H_2$-$N_2O$ mixtures [4]. The flame speeds of $H_2$-$N_2O$-Ar mixtures and $H_2$-$N_2O$-$N_2$ mixtures were investigated by Mével et al. [5] and Bane et al. [6], respectively. Mével et al. [7,8] and Javoy et al. [9] measured ignition delay times. Liang et al. [10] studied deflagration to detonation transition in undiluted $H_2$-$N_2O$ mixtures. Akbar et al. [11] and Kaneshige et al. [12] measured the detonation cell size and Zhang et al. [13] measured the critical energy required for direct detonation initiation. A number of other studies have also been performed on flammability limits, flame speed, and auto-ignition delay-time [5-8]. Despite these extensive studies, we are not aware of any data on the electrostatic discharge ignition potential for these mixtures. The objective of the present study is to characterize the energies needed for electrostatic discharge ignition of diluted and undiluted $H_2$-$N_2O$ mixtures. Experiments were performed for selected equivalence ratios, dilution levels, initial pressures, flanged and plain electrodes, and compared to a simple model of spark ignition.

## 2. Materials and Methods

### *2.1. Ignition System*

We have developed [16] a low-energy (60 μJ to 1.8 mJ), short duration (<50 ns) capacitive spark ignition system capable of producing 1.5 mm to 4 mm discharges with high repeatability. This

simulates the type of spark discharge encountered in typical electrostatic ignition hazards. The circuit consists of a 0-30 kV high voltage power supply connected to a 10 GΩ charging resistor in series with a 3-30 pF variable vacuum capacitor or a 15-250 pF variable vacuum capacitor. The capacitor is connected in parallel with the spark gap, so that it discharges through the gap when the capacitor reaches the gap breakdown voltage. A function generator provides a ramp signal to the high voltage power supply allowing it to ramp up from 0 to 10 kV. The ramp time is longer than the maximum capacitor charging time; therefore, the voltage on the capacitor at the time of breakdown can be measured at the output of the power supply. At breakdown, the spark current is measured using a Bergoz fast current transformer and triggers an oscilloscope that digitizes the output at a sampling rate of 2 GS/s. A 5 V output signal on the oscilloscope is then used to trigger a delay generator that triggers a high voltage relay, the data acquisition, and a high-speed camera. The high voltage relay is used to disconnect the capacitor from the high voltage power supply after the spark has occurred to prevent multiple sparks.

*2.2. Estimating Spark Energy*

The energy of the spark is approximated as the difference between the initial stored energy in the capacitor and the residual energy [16,17].

$$E_{spark} \approx E_{stored} - E_{residual} \quad . \tag{1}$$

The stored energy and residual energy are given by

$$E_{stored} = \frac{1}{2} C V_{breakdown}^2 \quad , \tag{2}$$

$$E_{residual} = \frac{1}{2} \frac{Q_{residual}^2}{C} \quad . \tag{3}$$

The total capacitance, $C$, is measured using a Keithley Model 6517A Electrometer/High Resistance Meter and the voltage at breakdown, $V_{breakdown}$, is measured using a high voltage probe. The residual charge, $Q_{residual}$, is found by subtracting the charge deposited into the spark channel from the stored charge in the capacitor. The integral of the spark current (equal to the charge deposited into the spark

channel) is found by numerically integrating the waveform obtained from the current transformer.

$$Q_{residual} = Q_{stored} - Q_{spark} \tag{4}$$

$$Q_{residual} = CV_{breakdown} - \int i(t)\,dt \tag{5}$$

The uncertainty in the spark energy measurement is calculated given the uncertainty in the voltage (4%), capacitance (3%) and current measurements (0.5%), which leads to an uncertainty of approximately 10% in the computed spark energy.

*2.3. Combustion Vessel and Diagnostics*

The ignition experiments were performed in a closed, cylindrical, stainless steel combustion vessel with a volume of approximately 22 L. Two parallel flanges were used to mount the spark gap electrodes, and two additional flanges held windows for visualization. A remotely controlled plumbing system is used to evacuate the chamber and accurately fill it with gases using the method of partial pressures. A Heise 901A manometer with a precise digital readout measures the static pressure so the gases can be filled to within 0.03% of the desired gas pressure, providing precise control over the mixture composition. Three different methods were used for ignition detection. First, the pressure rise from the combustion was measured using a pressure transducer. This measurement also allowed us to determine the peak pressure rise in the vessel. Second, the temperature rise was detected using a K-type thermocouple located inside the vessel. The third method used to detect ignition was schlieren visualization of the flame propagation recorded using a high-speed camera. Two different schlieren systems were used: the first had a large field of view (120 mm diameter) to visualize the flame propagation and the second had a small field of view (5.5 mm diameter) to visualize the early stages of the spark discharge and flame kernel development.

## 3. Results and discussion

Ignition tests were performed at ambient temperature for both undiluted and nitrogen-diluted $H_2$-$N_2O$ mixtures at an initial temperature of 298 K. The electrodes used in the tests were made of tungsten and were conical in shape with a base diameter of approximately 5 mm, cone angle of 8°, and a tip radius of approximately 0.25 mm. A Teflon flange, 13.5 mm in diameter and 1.6 mm thick, was

placed on the tip of each electrode leaving 1 mm of each tip exposed. Tests for all mixtures were performed with the flanges, and two additional test series were performed without the flanges. Ignition tests were performed over a range of spark lengths (1.5 – 4.0 mm), and based on our previous studies [16,17], the results were presented as spark energy densities (defined in this study as the spark energy divided by the spark gap distance) rather than as spark energies. The test results were analyzed using the statistical methods described in Bane [17], resulting in a probability distribution for ignition versus spark energy density. A typical waveform used to estimate the spark energy is shown in Fig. 1. The number of tests used to determine the probability distribution for each case was between 19 and 31. An example of the large field of view schlieren image sequence of the flame propagation of an $H_2$-$N_2O$ mixture with an equivalence ratio of 0.15 is shown in Fig. 2. A second example of a flame propagation in a $\phi = 0.2$ $H_2$-$N_2O$ mixture, is shown in Fig. 3; the Teflon flanges are visible on the electrode tips. In both cases, the initial temperature and pressure were 298 K and 20 kPa, respectively, with a camera framing rate of 6400 images per second. These cases were obviously both successful ignitions with a flame ultimately propagating away from the electrodes into the surrounding combustible mixture.

*3.1. Effect of Initial Conditions on MIE*

An example of the ignition test data at an equivalence ratio of 0.2 and a pressure of 25 kPa is shown with the resulting probability distribution in Fig. 4. The ignition and no ignition points overlap with the lowest ignition occurring at 81 μJ/mm and the highest no ignition occurring at 82 μJ/mm. This small overlap is reflected in the narrowness of the probability curve. The 95% confidence intervals and the data overlap region are also shown in Fig. 4. This case was exceptional in having a well-defined ignition threshold; our experience with other mixtures [16,17] is that there is substantial overlap between ignition and non-ignition cases and a significant dependence of ignition probability on ignition energy.

We carried out a series of tests to determine the ignition probability (Table 1) as a function of spark energy density for initial pressures of 15, 20, and 25 kPa (Fig. 5), equivalence ratios of 0.15 and 0.2

(Fig. 6), and dilutions of zero and 20% $N_2$ (Fig. 7). As discussed in the subsequent section, the ignition energy is predicted to increase with decreasing initial pressure and/or burning speed. Although the minimum spark energy density is not defined by the statistical model; the trend for the median spark energy density can be examined and shows a systematic dependence on pressure: 175 μJ/mm at 15 kPa; 98 μJ/mm at 20 kPa; 81 μJ/mm at 25 kPa. This is in reasonable agreement with the inverse pressure dependence of the model (Fig. 8). However, the greater extent of the overlap region, as evidenced by the slope of the distribution near the median value in Fig. 5, leads to large confidence intervals for the lower pressures and greater uncertainty in the median spark energy density. The laminar burning speeds [6] at $\phi = 0.15$ are 60% smaller than those at $\phi = 0.20$ and the ignition model, described in the subsequent section, predicts a strong dependence ($S_L^{-2}$) of ignition energy on laminar burning speed. However, the ignition probability curves are essentially identical (Fig. 6) for these two cases given that the 95% confidence intervals (not shown) at the median (114 μJ/mm for $\phi = 0.15$ and 98 μJ/mm for $\phi = 0.2$) are approximately the width of the distribution. The addition of 20% $N_2$ dilution has a more dramatic effect (Fig. 7) than changing the equivalence ratio; the median spark energy density is 98 μJ/mm for 0% dilution and 195 μJ/mm for 20% dilution. The confidence intervals are rather large for these cases and we do not have sufficient data to draw any conclusions about the validity of the trends. The range of parameters that we can explore experimentally is quite limited for these mixtures because at higher pressures and equivalence ratios, the ignition energies are too small (a few μJ) to measure and at higher dilutions and lower pressures, the quenching distances are too large to allow experimentation with reasonable gap lengths and breakdown voltages. In order to deal with these limitations, we have explored the utility of a simple ignition kernel model that can be used to extrapolate the present data.

*3.2. Comparison with Ignition Prediction Model*

Using the cylindrical kernel model [16], along with experimental laminar burning speed results from Bane et al. [6] and calculated laminar burning speeds from the Mével reaction mechanism [7,18], a prediction of the ignition energy density was made. The cylindrical kernel model, Eq. (8), assumes

that the flame kernel is a cylindrical volume of gas ignited by a linear spark. This model is based on the idea of a balance of the energy generated through the chemical reactions and the thermal energy lost to the surrounding cold gas through conduction

$$E_{density} = 12.6P\left(\frac{c_P}{R_b}\right)\left(\frac{T_b - T_u}{T_b}\right)\left(\frac{\alpha}{S_L}\right)^2 \tag{8}$$

where $\alpha$ is the thermal diffusivity, $R_b$ is the gas constant of the burned products and $T_u$ and $T_b$ are the temperatures of the unburned and burned gas, respectively. The laminar burning speed is defined as $S_L$. Shown in Fig. 8 is the 50% probability of ignition and the 95% confidence bounds from the $\phi$ = 0.2 $H_2$-$N_2O$ mixture ignition tests at various initial pressures along with the ignition predictions. The large differences between the two computed ignition energies is due to the difference in the laminar burning speeds used since the predicted ignition energy is proportional to $S_L^{-2}$. For example, at an equivalence ratio and initial pressure of 0.15 and 20 kPa, respectively, the experimental laminar burning speed and calculated laminar burning speed from the Mével model are 33 cm/s and 24.5 cm/s, respectively. As indicated in the Fig. 8, the cylindrical kernel model better matches the ignition energy results when using the experimental laminar burning speeds of the mixture. There is a 50%, 10% and 14% difference between the cylindrical kernel model using the experimental laminar burning speeds and the measured median ignition energy for $H_2$-$N_2O$ at initial pressures of 15 kPa, 20 kPa, and 25 kPa, respectively.

*3.3. Effect of Electrode Geometry on MIE*

It is well established that ignition energies are influenced [14,15,16] by the geometry of the electrodes and the addition of confining flanges. To examine the effect of flanges, ignition tests with and without flanged electrodes were performed at $\phi$ = 0.15 and 0.2 at an initial pressure of 20 kPa. The statistical analysis of the data is shown in Fig. 9. For $\phi$ = 0.15, the median ignition energy density for the flanged electrodes and plain electrodes was 114 μJ/mm and 144 μJ/mm, respectively. For $\phi$ = 0.2, the median ignition energy density for the flanged electrodes and plain electrodes was 98 μJ/mm and 90 μJ/mm. Using the flanged electrodes, testing was done at a flange spacing of 4.5 mm

for both equivalence ratios. Using the plain electrodes, testing was done at an electrode spacing of 3.0 mm and 4.0 mm for $\phi = 0.15$ and at an electrode spacing of 2.5 mm and 3.5 mm for $\phi = 0.2$. The quenching distances, $d_T$, are estimated [19] using

$$d_T = \frac{10\alpha}{S_L} \tag{9}$$

and for $H_2$-$N_2O$ at an initial pressure of 20 kPa and equivalence ratios of 0.15 and 0.2 these are 5.5 mm and 3.4 mm, respectively. This means that the present flanged tests are done under conditions where the gap is comparable to the quenching distance, the classical criterion [14,15] for determination of the so-called minimum ignition energy (MIE) as defined by Lewis and von Elbe [14]. The differences in the median spark energy density observed between the flanged and plain electrodes for the two equivalence ratios are modest and within the confidence band suggesting that the flanges have little influence on the ignition energy for these mixtures. This is consistent with the observations of Lewis and von Elbe [14] using plain electrodes and glass flanged electrodes, who found essentially identical values for MIE for the two cases for a range of gap sizes comparable to or larger than the quenching distance.

Images from the small field of view schlieren visualization of the spark discharge are shown in Fig. 10 for an $H_2$-$N_2O$ mixture with an equivalence ratio and initial pressure of 0.2 and 20 kPa, respectively, and the flanged and plain electrode configuration. The center of the initial flame kernel is predominantly cylindrical; and as a result of the tips of the electrodes being exposed, the wave is spherical near the electrodes. The development of the flame up until 51 μs is almost identical in the two cases, consistent with our observations that flanges have little influence on ignition energy for these cases.

## 4. Conclusion

In the present study, the electrostatic ignition energies of selected $H_2$-$N_2O$ mixtures have been characterized through experimental measurements of the ignition probability. We found that a cylindrical kernel model is a useful guideline for predicting the median ignition energy of $H_2$-$N_2O$ as

long as experimental burning speeds are used. Using this model, results from this study can be extrapolated to estimate the median ignition energies of $H_2$-$N_2O$ at higher pressures where potential explosion hazards are often considered. According to Bane et al. [7], the laminar burning speed of $H_2$-$N_2O$ is independent of pressure over a large range; therefore for a given composition, the median ignition energy density will be approximately $E_{den} \sim P^{-1}$. For $H_2$-$N_2O$ at an initial pressure of 100 kPa and equivalence ratio of 0.2, the estimated ignition energy density is 20 μJ/mm and an ignition energy density of less than 1 μJ/mm is predicted for stoichiometric $H_2$-$N_2O$ at an initial pressure of 100 kPa. This value is comparable to or less than the ignition energy density of $H_2$-$O_2$, which is approximately equal to 5-10 μJ/mm, at similar conditions [20]. These results suggest than the potential for electrostatic spark discharge ignition of $H_2$-$N_2O$ mixtures is comparable to or greater than that of $H_2$-$O_2$ mixtures.

## References


1. **M.S. Gerber**, Legend and legacy: fifty years of defense production at the Hanford site. Tech. Rep. WHC-Re0293-Rev.2. Westinghouse Hanford Co, 1992.

2. **N.D. Lichtenstein**, Nat. Resour. J. 44 (2004) 809-839.

3. **L.A. Mahoney, J.L. Huckaby, S.A. Bryan and G.D. Johnson**, Overview of the flammability of gases generated in Hanford waste tanks. Tech. Rep. PNNL-13269. Richland, Wash: Pac Northwest Nat Lab, 2000.

4. **U. Pfahl, M. Ross and J. Shepherd**, Combust. Flame 123 (2000) 140-158.

5. **R. Mével, F. Lafosse, N. Chaumeix, G. Dupré and C. E. Paillard**, Int. J. Hydrogen Energy 34 (2009) 9007-9018.

6. **S. P. M. Bane, R. Mével, S.A. Coronel and J.E. Shepherd**, Int. J. Hydrogen Energy 36 (2011) 10107-10116.

7. **R. Mével, S. Javoy, F. Lafosse, N. Chaumeix, G. Dupré and C. E. Paillard**, Proc. Combust. Inst. 32 (2009) 359-366.

8. **R. Mével, F. Lafosse, L. Catoire, N. Chaumeix, G. Dupré and C.E. Paillard**, Combust. Sci. and Tech. 180 (2008).

9. **S. Javoy, R. Mével and C. E. Paillard**, Int. J. Chem. Kinet. 41 (2009) 357-375.

10. **Z. Liang, J. Karnesky and J. Shepherd**, Structural response to reflected detonation and deflagration-to-detonation transition in $H_2$-$N_2O$. GALCIT rep. FM2006-003, California Institute of Technology, 2006.

11. **R. Akbar, M. Kaneshige, E. Schultz and J.E. Shepherd**, Detonations in $H_2$-$N_2O$-$CH_4$-$NH_3$-$O_2$-$N_2$ mixtures. GALCIT rep. FM97-3, California Institute of Technology, 1997.

12. **M. Kaneshige, E. Schultz, U. Pfahl, J. Shepherd and R. Akbar**, Proc 22nd Int. Symp. Shock Waves 1 (2000) 251-256.

13. **B. Zhang, H.D. Ng, R. Mével and J.H.S. Lee**, Int. J. Hydrogen Energy 36 (2011) 5707-5716.

14. **B. Lewis and G. V. Elbe**, Combustion, Flames, and Explosions of Gases, Academic Press, New York, 1961

15. **M. F. Calcote, C. A. Gregory, Jr., C. M. Barnett and R. B. Giemer**, Indus. Engin. Chem. 44 (1952) 2656–2662.

16. **S. P. M. Bane,** Spark Ignition: Experimental and numerical investigation with application to aviation safety. Ph.D. thesis, California Institute of Technology, 2010.

17. **S. P. M Bane, J. E. Shepherd, E. Kwon, and A. C. Day,** Int. J. Hydrogen Energy 36 (2011) 2344-2350.

18. **R. Mével, S. Javoy and G. Dupré,** Proc. Combust. Instit. 33 (2011) 485–492.

19. **D. R. Ballal and A. H. Lefebvre**, Proc. R. Soc. Lond. A. 357 (1977) 163-181.

20. **E. L. Litchfield**, Minimum ignition-energy concept and its application to safety engineering. Bureau of Mines rep. 5671, U.S. Dept. of the Interior, Bureau of Mines, 1960.

# Tables

Table 1
Probability of ignition

| Pressure (kPa) | $\phi$ | % $N_2$ | Electrode configuration | 50% probability of ignition (mJ/mm) | Confidence bounds (mJ/mm) |
|---|---|---|---|---|---|
| 15 | 0.2 | 0 | Flanged | 175 | 86 - 264 |
| 20 | 0.15 | 0 | Flanged | 114 | 82 - 147 |
| 20 | 0.15 | 0 | Plain | 143 | 95 - 193 |
| 20 | 0.2 | 0 | Flanged | 98 | 67 - 129 |
| 20 | 0.2 | 0 | Plain | 90 | 73 - 106 |
| 20 | 0.2 | 20 | Flanged | 195 | 133 - 257 |
| 25 | 0.2 | 0 | Flanged | 81 | 77 - 86 |

# Figures

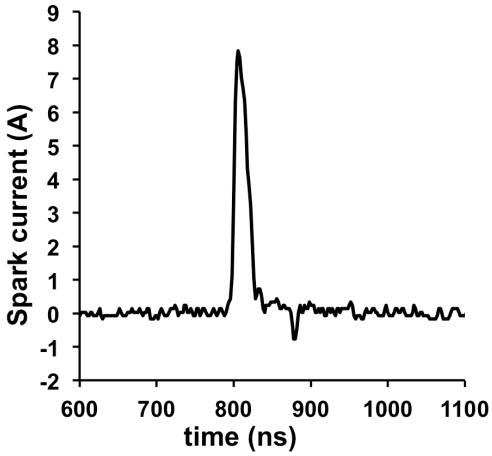


Figure 1. Current waveform ($C$ = 55 pF) of spark with breakdown voltage of 3.8 kV

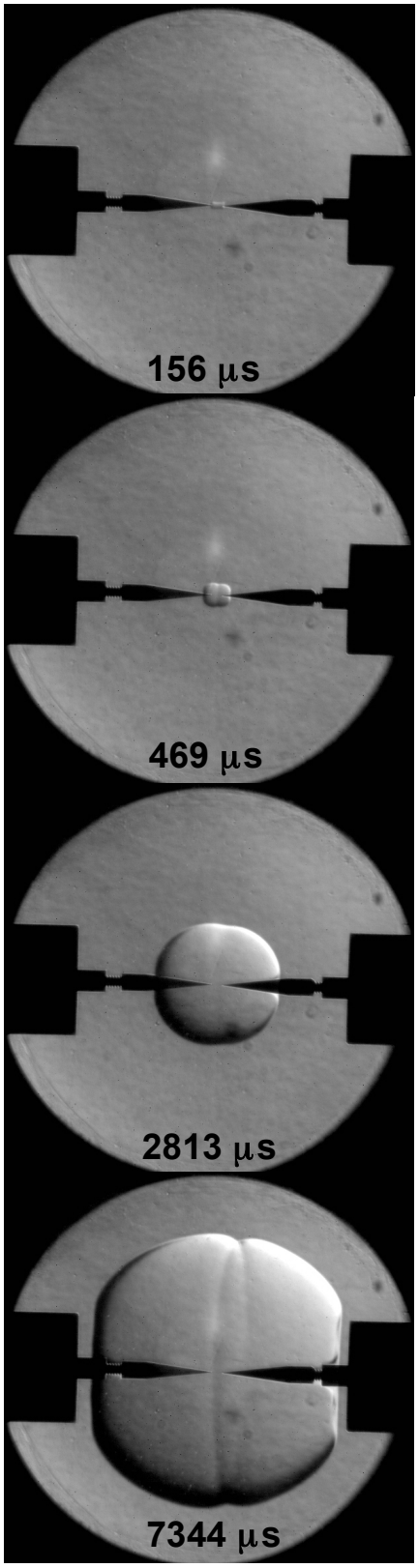


Figure 2. Example of a schlieren image sequence of flame propagation in a $\phi = 0.15$ $H_2$-$N_2O$ mixture with an initial pressure of 20 kPa and no flanges on the electrode tips. The field of view has a diameter of approximately 11.7 cm.

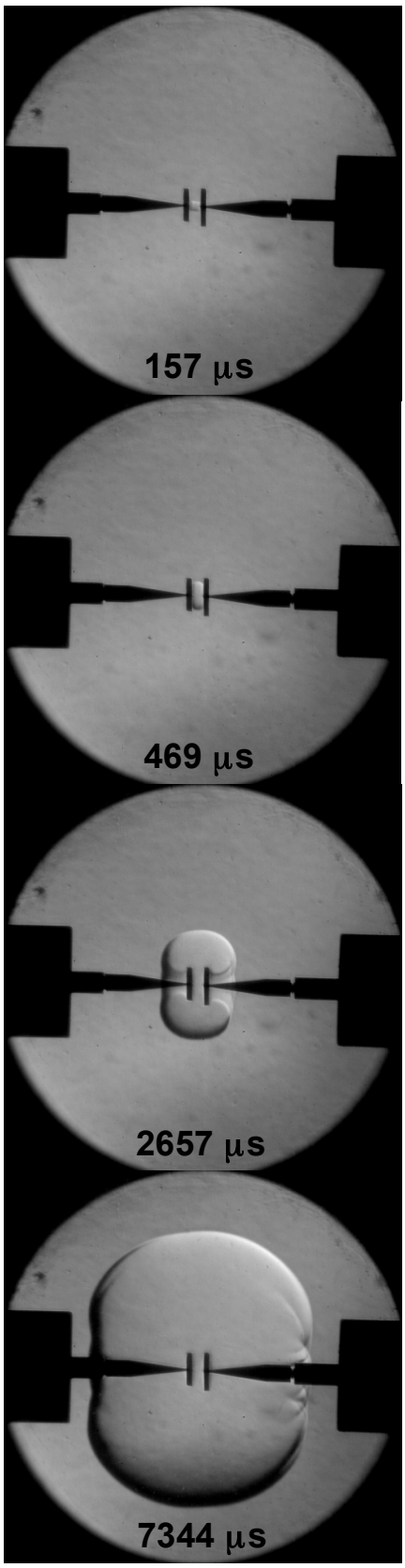


Figure 3. Example of a schlieren image sequence of flame propagation in a $\phi = 0.2$ $H_2$-$N_2O$ mixture with an initial pressure of 20 kPa with Teflon flanges on the electrode tips. The field of view has a diameter of approximately 11.7 cm.

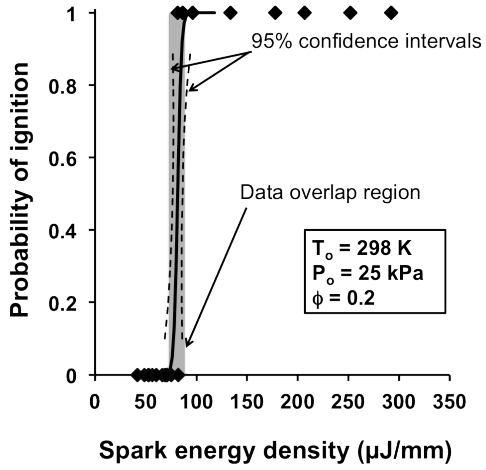


Figure 4. Probability distribution versus spark energy density for an $H_2$-$N_2O$ mixture at an initial pressure of 25 kPa and $\phi = 0.2$. Shown as dashed lines are the 95% confidence intervals and in gray is the data overlap region.

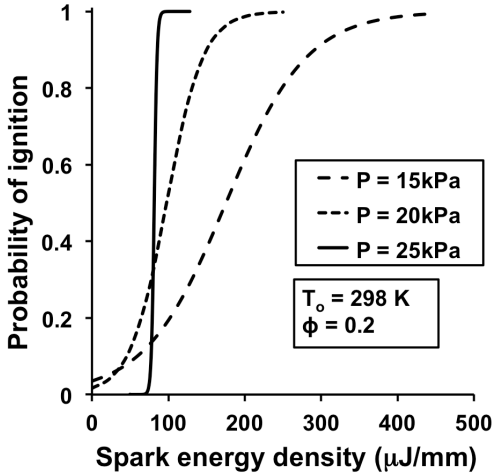


Figure 5. Effect of initial pressure on the ignition probability distribution of $H_2$-$N_2O$ at $\phi = 0.2$.

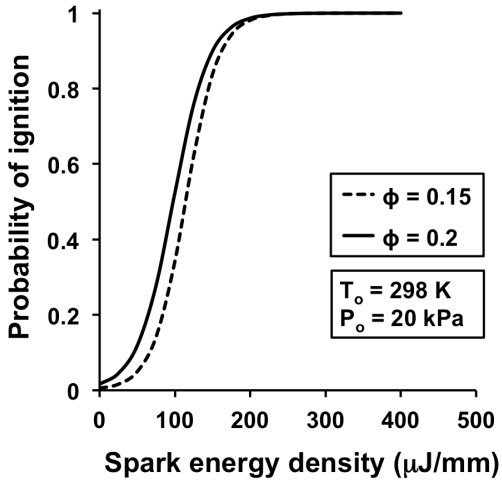


Figure 6. Effect of equivalence ratio on the ignition probability distribution of $H_2$-$N_2O$ at an initial pressure of 20 kPa.

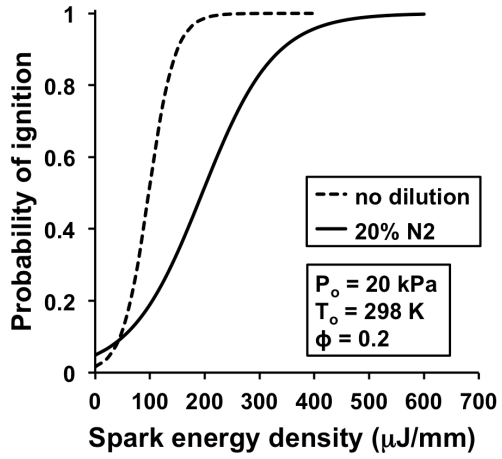


Figure 7. Effect of $N_2$ dilution on the ignition probability distribution of $H_2$-$N_2O$-$N_2$ at an initial pressure of 20 kPa and $\phi = 0.2$.

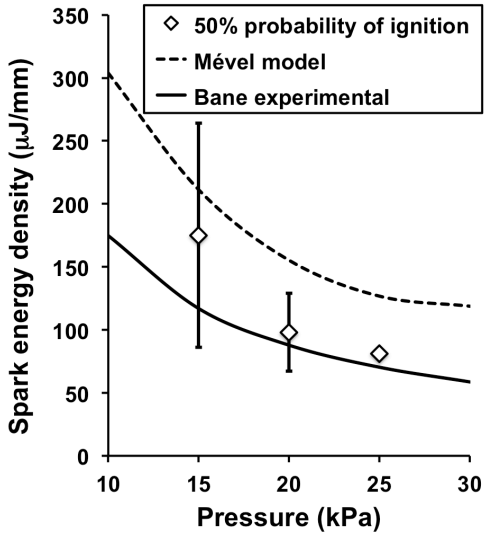


Figure 8. Estimated MIE using the cylindrical kernel model [16] with the Mével model for laminar burning speed predictions, or experimental laminar burning speeds [6] compared with energies for 50% probability of ignition from the present study.

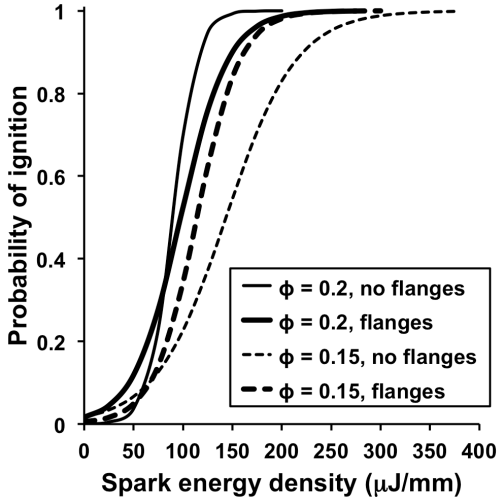


Figure 9. Effect of electrode geometry on the ignition probability distribution of $H_2$-$N_2O$-$N_2$ at an initial pressure of 20 kPa and $\phi$ = 0.15 and 0.2.

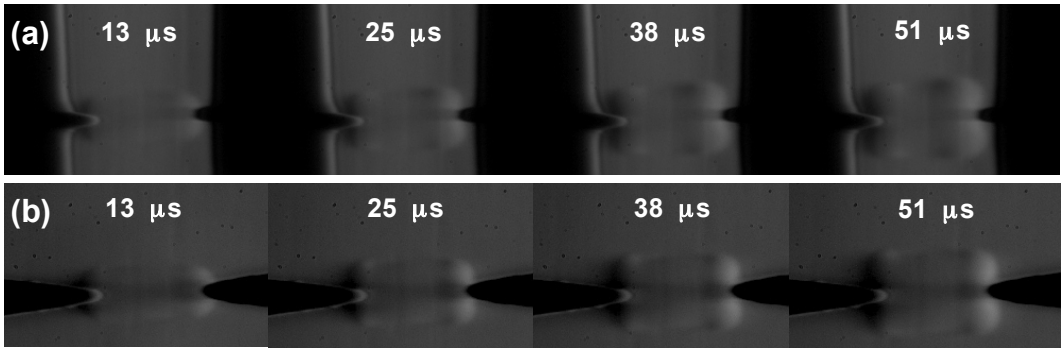


Figure 10. Schlieren image sequence of initial kernel formation in a $\phi = 0.2$ $H_2$-$N_2O$ mixture with an initial pressure of 20 kPa and electrode gap of 2.5 mm. (a) Flanged electrodes, (b) plain electrodes.

# Captions

Table 1: Probability of ignition

Figure 1. Current waveform ($C$ = 55 pF) of spark with breakdown voltage of 3.8 kV

Figure 2. Example of a schlieren image sequence of flame propagation in a $\phi = 0.15$ $H_2$-$N_2O$ mixture with an initial pressure of 20 kPa and no flanges on the electrode tips. The field of view has a diameter of approximately 11.7 cm.

Figure 3. Example of a schlieren image sequence of flame propagation in a $\phi = 0.2$ $H_2$-$N_2O$ mixture with an initial pressure of 20 kPa with Teflon flanges on the electrode tips. The field of view has a diameter of approximately 11.7 cm.

Figure 4. Probability distribution versus spark energy density of $H_2$-$N_2O$ at an initial pressure of 25 kPa and $\phi = 0.2$. Shown as dashed lines are the 95% confidence intervals and in gray is the data overlap region.

Figure 5. Effect of initial pressure on the ignition probability distribution of $H_2$-$N_2O$ at $\phi = 0.2$.

Figure 6. Effect of equivalence ratio on the ignition probability distribution of $H_2$-$N_2O$ at an initial pressure of 20 kPa.

Figure 7. Effect of $N_2$ dilution on the ignition probability distribution of $H_2$-$N_2O$-$N_2$ at an initial pressure of 20 kPa and $\phi = 0.2$.

Figure 8. Estimated MIE using the cylindrical kernel model [16] with the Mével model for laminar burning speed predictions, or experimental laminar burning speeds [6] compared with energies for 50% probability of ignition from the present study.

Figure 9. Effect of electrode geometry on the ignition probability distribution of $H_2$-$N_2O$-$N_2$ at an initial pressure of 20 kPa and $\phi = 0.15$ and 0.2.

Figure 10. Schlieren image sequence of initial kernel formation in a $\phi = 0.2$ $H_2$-$N_2O$ mixture with an initial pressure of 20 kPa. (a) Flanged electrodes, (b) plain electrodes.